Full Paper
doi.org/10.1002/chem.202003214

Polymorphism

Synthesis-Controlled Polymorphism and Optical Properties of Phyllosilicate-Analogous Borosulfates $M[B_2(SO_4)_4]$ (M = Mg, Co)

Philip Netzsch,[a] Florian Pielnhofer,[b] Robert Glaum,[c] and Henning A. Höppe*[a]

Dedicated to Prof. Harald Hillebrecht on the occasion of his 60th birthday

Abstract: Increased synthetic control in borosulfate chemistry leads to the access of various new compounds. Herein, the polymorphism of phyllosilicate-analogous borosulfates is unraveled by adjusting the oleum (65% SO_3) content. The new polymorphs β-$Mg[B_2(SO_4)_4]$ and α-$Co[B_2(SO_4)_4]$ both consist of similar layers of alternating borate and sulfate tetrahedra, but differ in the position of octahedrally coordinated cations. The α-modification comprises cations between the layers, whereas in the β-modification cations are embedded within the layers. With this new synthetic approach, phase-pure compounds of the respective polymorphs α-$Mg[B_2(SO_4)_4]$ and β-$Co[B_2(SO_4)_4]$ were also achieved. Tanabe–Sugano analysis of the Co^{2+} polymorphs reveal weak ligand field splitting and give insights into the coordination behavior of the two-dimensional borosulfate anions for the first time. DFT calculations confirmed previous in silico experiments and enabled an assignment of the polymorphs by comparing the total electronic energies. The compounds are characterized by single-crystal XRD, PXRD, FTIR, and UV/Vis/NIR spectroscopy, thermogravimetric analysis (TGA), and density functional theory (DFT) calculations.

Introduction

During recent years, borosulfates have gained interest as new representatives of silicate-analogous materials. Built up by corner-sharing borate and sulfate tetrahedra,[1] their most common supertetrahedral fundamental building unit $[B(SO_4)_4]^{5-}$ shows a further analogy towards silicates: the boron atom can be considered as a tetrahedral center T and the sulfate tetrahedra as terminal or bridging moieties *X*. Consequently, most borosulfates can be structurally derived from these supertetrahedra TX_4. Thus, compounds solely comprising alternating borate and sulfate tetrahedra by corner- or edge-sharing supertetrahedra are classified as classic borosulfates. In accordance with the great structural diversity of silicates,[2] borosulfates also exhibit several connection patterns consisting of zero-dimensional anions in $K_5[B(SO_4)_4]$ (composition of the anion TX_4),[3] one-dimensional chains in $K_3[B(SO_4)_3]$ (TX_3),[4] two-dimensional layers in $Ca[B_2(SO_4)_4]$,[5] or three-dimensional networks in $Li[B(SO_4)_2]$ (TX_2).[4] In addition to this, also unconventional borosulfates comprising B-O-B-bridges[6] or S-O-S-bridges occur.[7]

As the amount of new borosulfates increases rapidly,[1] the lack of knowledge about their properties becomes an increasingly important topic. In particular, their optical properties are of interest, as silicate-analogous materials often provide excellent host structures for doping with Eu^{2+}, Ce^{3+}, or other transition metal ions, such as phosphor materials.[8] Therefore, compounds consisting of optically active ions, like the aforementioned transition metal ions are of great significance for assessing new insights into the coordination behavior. Our first investigations addressed the transition metal borosulfates $M_4[B_2O(SO_4)_6]$ (M = Mn, Co, Ni, Zn),[9] structurally related to the silicophosphates $A_4[Si_2O(PO_4)_6]$ (A = Ti, V, Cr, Mo).[10] Herein, the metal cations form M_2O_9 dimers of face-sharing octahedra, coordinated by oxygen atoms stemming from zero-dimensional $[B_2O(SO_4)_6]^{8-}$ anions (T_2OX_6). A Tanabe–Sugano analysis of the absorption spectra of the cobalt and nickel compounds revealed values for the ligand field splitting Δ_O and the Racah parameter *B* comparable to the respective transition metal sulfates or chlorides.[9] Additionally, we characterized the rare-earth borosulfates $R_2[B_2(SO_4)_6]$ (R = Y, La–Lu, except Pm), com-

[a] P. Netzsch, Prof. Dr. H. A. Höppe
Lehrstuhl für Festkörperchemie
Universität Augsburg
Universitätsstr. 1, 86159 Augsburg (Germany)
E-mail: henning.hoeppe@physik.uni-augsburg.de

[b] Dr. F. Pielnhofer
Institut für Anorganische Chemie
Universität Regensburg
Universitätstr. 31, 93053 Regensburg (Germany)

[c] Prof. Dr. R. Glaum
Institut für Anorganische Chemie
Universität Bonn
Gerhard-Domagk-Str. 1, 53121 Bonn (Germany)

Supporting information and the ORCID identification number(s) for the author(s) of this article can be found under:
https://doi.org/10.1002/chem.202003214.

prising zero-dimensional cyclic $[B_2(SO_4)_6]^{6-}$ anions. The photoluminescence spectra for the cerium, europium, and terbium compounds showed similarities to the respective rare earth metal fluorides.[11] Thus, the knowledge of optical properties is so far solely based on borosulfates comprising zero-dimensional anions.

The reason for this is that highly condensed structures are in general still little-known for borosulfates. Besides the only three-dimensional borosulfate framework in $Li[B(SO_4)_2]$,[4] only a few borosulfates with two-dimensional networks have been structurally characterized. These can be classified as unconventional borosulfates such as $B_2O(SO_4)_2$[12] and $Cs[B_2O(SO_4)_3]$[6c] or classic borosulfates such as $Mg[B_2(SO_4)_4]$[9] and $Ca[B_2(SO_4)_4]$.[5] Very recently, also transition metal borosulfates $M[B_2(SO_4)_4]$ (M = Mn, Co, Ni, Zn) were described.[13] Although they comprise homeotypic anionic layers, the crystal structures differ from each other by the location of the cation relative to the layered anion. In $M[B_2(SO_4)_4]$ (M = Mg, Ni), the cations are located between the layers, whereas in $M[B_2(SO_4)_4]$ (M = Mn, Co, Zn) they occupy positions within the layer.[9,13] Based on in silico experiments, the authors propose that cobalt and zinc also should form isotypic structures to $Mg[B_2(SO_4)_4]$.[13b] Yet, polymorphism is very scarce in borosulfates. Up to now, this has only been observed for $Na_5[B(SO_4)_4]$[4] and $Mg_4[B_2O(SO_4)_6]$.[9] In both cases, however, only one polymorph could be synthesized phase purely.

With respect to phyllosilicate-analogous borosulfates, the synthesis remains challenging. Hitherto, only a few single crystals were obtained for $Mg[B_2(SO_4)_4]$[9] and the transition metal borosulfates $M[B_2(SO_4)_4]$ (M = Mn, Co, Ni, Zn) could not be obtained as phase-pure powders—except for $Zn[B_2(SO_4)_4]$.[13] However, phase-pure powders are a precondition for reliable property measurements. Moreover, a selective access to the respective modification was not reported, however.

Herein, we describe the synthesis-controlled polymorphism in $M[B_2(SO_4)_4]$ (M = Mg, Co)—yielding phase-pure samples of all polymorphs. We characterize these polymorphs by single-crystal (SC)-XRD, PXRD, IR spectroscopy, and thermal analysis and compare stabilities of the polymorphs based on DFT calculations. Furthermore, Tanabe–Sugano analysis was performed for the cobalt polymorphs, yielding optical properties for two-dimensional borosulfates for the very first time.

Results and Discussion

Synthetic approach

All compounds were synthesized solvothermally at 180 °C in torch-sealed silica glass ampoules starting from the respective metal carbonates $MgCO_3$ and $CoCO_3{\cdot}H_2O$ and boron oxide B_2O_3. The applied ratio between sulfuric acid and oleum (65% SO_3) turned out to be a crucial factor for accessing the chemically only slightly different polymorphs. Starting from pure oleum (1 mL), β-$M[B_2(SO_4)_4]$ (M = Mg, Co) was obtained as a phase-pure powder containing single crystals (Figure S1 b, d in the Supporting Information). Reducing the oleum fraction to equal amounts of oleum (0.5 mL) and sulfuric acid (0.5 mL) yielded phase purely the α-modification as single crystals (Figure S1 a, c in the Supporting Information).

However, in some cases, the β-modification was obtained instead of the α-modification even with equal amounts of sulfuric acid and oleum. Similar observations were made by using a lower fraction of oleum (0.4 mL with 0.6 mL H_2SO_4), whereas a further reduction to solely 0.3 mL oleum (with 0.7 mL H_2SO_4) prevented any crystallization under these conditions. Thus, the reduction of the oleum fraction promotes but does not guarantee the synthesis of the α-modification. To shift the system towards the exclusive formation of the α-modification, the prepared ampoule with equal amounts of concentrated sulfuric acid and oleum was additionally left standing at room temperature for one day before thermal treatment. Indeed, this change of synthesis conditions including an aging of the mother liquor yielded solely the α-modification.

After aging, the α-modification forms, comprising borosulfate layers separated by the charge compensating cations. Contrarily, in the β-modification, the cations are hosted within the layers. We suggest that the borosulfate layers therein are most likely formed directly around the cations during the initial stages of condensation and in the presence of free SO_3. So, apparently, the aging provides time to eject the cations from the layers to the inter-layer space—making these layers somewhat denser and reducing their surface. This coincides nicely with previous observations according to which the sulfate tetrahedra shift towards the surface on their quest to minimize the overall layer surface.[12]

Looking at the different ratios of oleum and sulfuric acid, a very similar story evolves: the less free SO_3 is available, the stronger is apparently the need to minimize the layer surface, promoting the α-modification already at early stages of the crystallization—the aging ensures that exclusively this modification is formed. Accordingly, the ratio of sulfuric acid and oleum, that is, the amount of available SO_3, as well as the aging are the two dominating figures to be considered for such selective syntheses.

We confirmed the phase purity for all compounds by Rietveld refinements on X-ray powder diffraction data (Figure 1).

Crystal structures

α-$Co[B_2(SO_4)_4]$ crystallizes in space group $C2/c$ (no. 15) isotypically with $Mg[B_2(SO_4)_4]$.[9] We classify this structure as α-$Mg[B_2(SO_4)_4]$ based on the lower total electronic energies compared with the β-polymorph. The densities of the respective phases determined by single-crystal X-ray diffraction are in line with Ostwald's rule although the DFT data do not show that trend, but—on the other hand—deliver more reliable results confirming the relative stabilities. The structure comprises infinite anionic layers parallel to the (1 0 0) plane (Figure 2). They consist of alternating, corner-sharing borate and sulfate tetrahedra and hence obey Loewenstein's rule.[14] Each borate tetrahedron bridges four adjacent sulfate tetrahedra, whereas the sulfate tetrahedra have two bridging oxygen atoms towards borate tetrahedra and two terminal oxygen atoms. The respective bond lengths are in accordance with previously reported

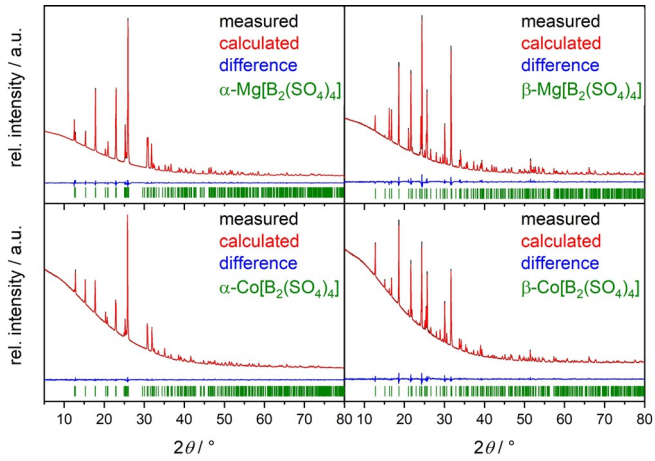

Figure 1. Rietveld refinement of α- and β-$M[B_2(SO_4)_4]$ (M = Mg, Co); measured (black line) and calculated (red line) powder diffraction pattern; theoretical reflection positions (green vertical bars) and the difference plot (blue line).

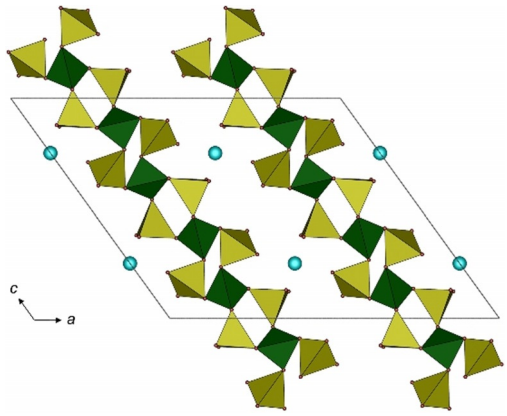

Figure 2. Unit cell of α-$Co[B_2(SO_4)_4]$ viewed along (0 1 0); borate tetrahedra green, sulfate tetrahedra yellow, cobalt cations cyan.

borosulfates[5,9,15] with shorter S–O bonds for the terminal oxygen atoms and comparatively longer ones for the bridging oxygen atoms (Table 1). The tetrahedra can be classified as regular ones as the deviation from the tetrahedral symmetry is −0.38 and −0.25 % for the sulfate tetrahedra and −0.47 % for the borate tetrahedron.[16]

According to Liebau's nomenclature of silicates,[2] the anion has phyllosilicate topology with *vierer* and *zwölfer* rings. By regarding the supertetrahedron $B(SO_4)_4$ as a building unit, each supertetrahedron TX_4 is connected to a further supertetrahedron by a common edge (e = edge-sharing) and to two additional supertetrahedra by common corners (c = corner-sharing) forming *sechser* rings (Figure 6 b, d). Thus, the anionic layer can be described by the Niggli formula $_\infty^2\{[B(SO_4)^e_{2/2}(SO_4)^c_{2/2}]^-\}$. As the structure comprises the connection pattern of the three-dimensional network like in *cristobalite* SiO_2[17] and one-dimensional chains like in SiS_2,[18] the B/S ratio of 1:2 results in a two-dimensional layer. The terminal oxygen atoms of the sulfate tetrahedra point towards the surface of the layers to coordinate the charge-compensating Co^{2+} ions, which separate the layers from each other. They are coordinated octahedrally by three oxygen atoms from the two adjacent layers (Figure 3). The Co–O distances of 204.18(13)–208.89(13) pm are well in accordance with the sum of the ionic radii (Σr_{ion} = 210 pm).[19] The coordination environment, as well as electrostatic consistency were confirmed by calculations based on the MAPLE concept[20] (Tables S8–S10 in the Supporting Information).

β-$M[B_2(SO_4)_4]$ (M = Mg, Co) crystallizes isotypically with $Zn[B_2(SO_4)_4]$[13a] in space group $P2_1/n$ (no. 14) with two formula units per unit cell (Figure 4). Similar to the α-modification, the structure consists of alternating corner-sharing borate and sulfate tetrahedra forming adjacent *vierer* and *zwölfer* rings within a layer spreading along the (1 0 1) plane. Hence, the edge- and corner-sharing supertetrahedra can be described by the Niggli formula $_\infty^2\{[B(SO_4)^e_{2/2}(SO_4)^c_{2/2}]^-\}$ in the β modification as well.

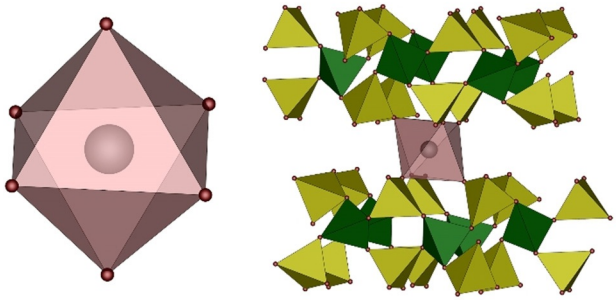

Figure 3. Octahedral coordination environment of the Co^{2+} ions (left) and the location of those octahedra between two adjacent layers (right) in α-$Co[B_2(SO_4)_4]$.

Table 1. Selected interatomic distances (in pm) and angles (in °) in the compounds α-$Co[B_2(SO_4)_4]$ and β-$M[B_2(SO_4)_4]$ (M = Co, Mg) (esds in parentheses).

	α-$Co[B_2(SO_4)_4]$	β-$Co[B_2(SO_4)_4]$	β-$Mg[B_2(SO_4)_4]$
M–O	204.18(13)–208.89(13)	205.27(15)–212.33(14)	202.77(11)–208.28(10)
Av. *M*–O	207.3	209.4	205.8
Σr_{ion}(M-O)[19]	210	210	207
S–O_{br}	151.86(12)–154.06(12)	152.15(12)–154.31(14)	151.10(11)–153.23(11)
S–O_{term}	141.21(13)–144.50(12)	142.36(14)–145.55(13)	142.46(11)–144.17(12)
B–O	145.29(19)–148.68(19)	146.00(19)–150.0(2)	144.55(18)–148.62(19)
O-*M*-O	87.13(6)–94.34(6)	84.54(6)–95.46(6)	86.06(4)–93.94(4)
O-S-O	100.82(7)–117.50(8)	97.69(6)–116.16(8)	97.49(6)–116.49(8)
O-B-O	106.88(13)–112.20(11)	101.19(11)–114.69(12)	101.24(11)–114.59(12)

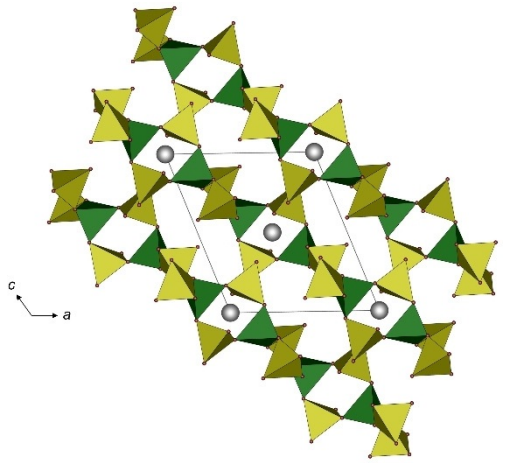

Figure 4. Unit cell of β-$Mg[B_2(SO_4)_4]$ viewed along (0 1 0); borate tetrahedra green, sulfate tetrahedra yellow, magnesium cations gray.

Therein, the sulfate tetrahedra deviate between −0.49 to −0.13% (Co) and −0.49 to −0.16% (Mg) from the tetrahedral symmetry,[16] the borate tetrahedra deviate −1.25% (Co) and −1.17% (Mg) and thus, all tetrahedra can be classified as regular ones. Unlike the α-modification, one of the terminal oxygen atoms of the sulfate tetrahedra point into the *zwölfer* ring and the other one off the layer surface.

The cations M^{2+} are situated on the corners and the center of the unit cell (Wyckoff site 2*a*). Consequently, the octahedral coordination of the M^{2+} cations is made up by a square planar coordination within the *zwölfer* ring and two oxygen atoms from adjacent layers leading to in total three involved layers per coordination sphere (Figure 5). This is in contrast to

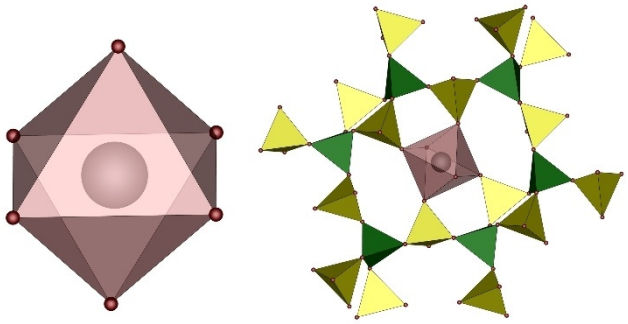

Figure 5. Octahedral coordination environment of the Mg^{2+} ions in β-$Mg[B_2(SO_4)_4]$ (left) and the location of those octahedra in the *zwölfer* ring with the two additional oxygen atoms stemming from the adjacent layers (right).

$Ca[B_2(SO_4)_4]$[5] and α-$Mg[B_2(SO_4)_4]$,[9] where the coordination environments involve only two layers. The resulting Co–O distances of 205.27(15)–212.33(14) pm and Mg–O distances of 202.77(11)–208.28(10) pm, respectively, are in agreement with the sum of the ionic radii (Σr_{ion}(Co-O) = 210 pm and Σr_{ion}(Mg-O) = 207 pm).[19] The coordination environment as well as electrostatic consistency of the structure model were confirmed by calculations based on the MAPLE concept[20] (Tables S8, S10, S11 in the Supporting Information).

Both structures, the α- and the β-modification, show silicate-analogous topologies. Although to the best of our knowledge, solely *vierer* and *zwölfer* rings next to each other have not been observed so far in silicates, the structure of manganpyrosmallite $Mn_8[Si_6O_{15}](OH, Cl)_{10}$ shows both in addition to the *sechser* rings, dominating the crystal structure.[21] Considering the above-mentioned supertetrahedral network, an astonishing similarity to hp-NiB_2O_4 can be found, where layers of edge- and corner-sharing borate tetrahedra are present (Figure 6).[22]

DFT calculations

To compare the stabilities of α-*M*$[B_2(SO_4)_4]$ and β-*M*$[B_2(SO_4)_4]$ (*M* = Mg, Co), the total electronic energies for the polymorphs of both compounds were calculated by means of density functional theory (DFT). The cell volumes for the probed structures are slightly overestimated by dispersion-corrected PBE-D3 calculations (α-$Mg[B_2(SO_4)_4]$: +6.2%; β-$Mg[B_2(SO_4)_4]$: +5.7%; α-$Co[B_2(SO_4)_4]$: +5.4%; β-$Co[B_2(SO_4)_4]$: +4.9%). Although a different basis set and xc-functional was used, the lattice parameters and cell volume for β-$Co[B_2(SO_4)_4]$ are in good agreement with the recent reported values.[13b] Bruns et al. have modelled the structures of the second polymorph for both *M*$[B_2(SO_4)_4]$ (*M* = Mg, Co). They find that a "cation between layer", which we denote as the α-polymorph, is energetically preferred over a "cation within layer", which we classify as the β-polymorph, by 27.7 kJ mol^{-1}. Both Mg polymorphs exhibit almost identical densities, which is confirmed by optimizing the structures and calculating energy versus volume plots (see Table 2). The divalent cation situated between the layers is confirmed to be more stable for $Mg[B_2(SO_4)_4]$ (see Figure 7), although the energy difference obtained with PBE-D3 is smaller (13 kJ mol^{-1}). Further, the calculated bulk modulus B_0 displays slightly less compressibility of the β-modification.

Based on the optical properties and our previous contribution on transition metal borosulfates,[9] a high-spin state was modelled for both $Co[B_2(SO_4)_4]$ polymorphs, which was con-

Table 2. Experimentally determined structural parameters (rounded to two decimal places, details in Table S7 in the Supporting Information) from Rietveld refinement from α- and β-*M*$[B_2(SO_4)_4]$ (*M* = Mg, Co) in comparison with the calculated structural parameters obtained with the PBE-D3.

	α-$Mg[B_2(SO_4)_4]$		β-$Mg[B_2(SO_4)_4]$		α-$Co[B_2(SO_4)_4]$		β-$Co[B_2(SO_4)_4]$	
	Exp.	PBE-D3	Exp.	PBE-D3	Exp.	PBE-D3	Exp.	PBE-D3
a [pm]	1747.49	1793.1	791.00	797.9	1742.54	1778.2	788.92	791.0
b [pm]	531.63	542.6	808.15	829.6	533.97	542.3	810.42	834.5
c [pm]	1430.96	1463.5	903.76	927.8	1432.14	1466.6	904.09	924.6
β [°]	126.34	126.74	111.37	111.78	126.03	126.33	111.29	111.86
V/Z [10^6 pm]	267.70	285.26	269.01	285.16	269.40	284.86	269.29	283.07

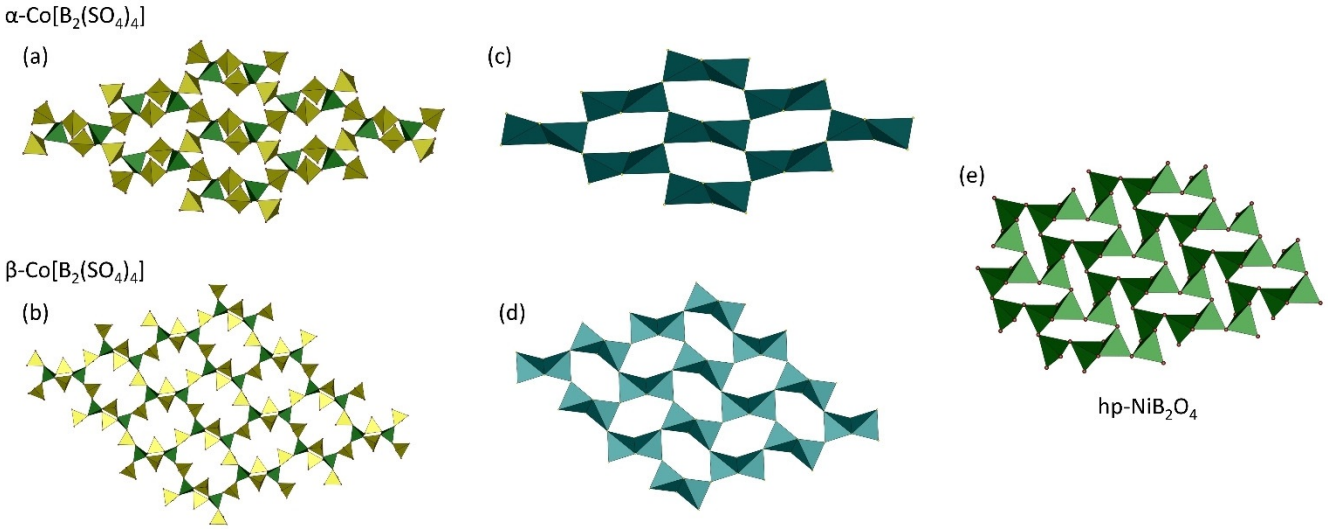

Figure 6. Tetrahedral layers in α- (a) and β-Co$[B_2(SO_4)_4]$ (b), layers build up by supertetrahedra (in turquoise) in α- (c) and β-Co$[B_2(SO_4)_4]$ (d) and the borate tetrahedral layers in hp-NiB_2O_4 (e).

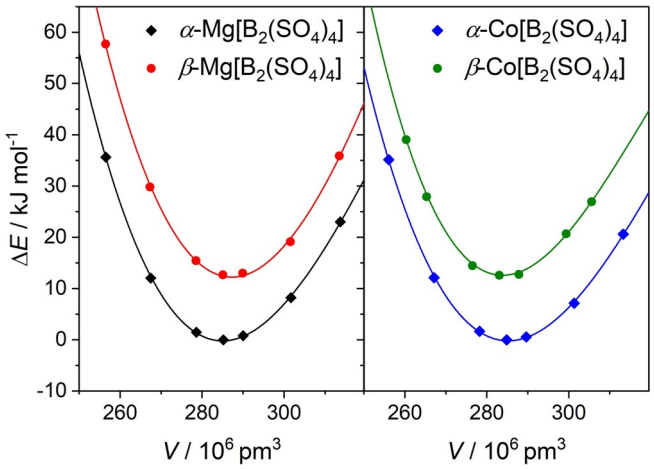

Figure 7. Energy vs. volume plots of α-$M[B_2(SO_4)_4]$ and β-$M[B_2(SO_4)_4]$ (M = Mg, Co).

firmed very recently by magnetic properties.[13b] Bruns et al. optimized both the experimental structure ("cation within layer") and a model isotypic to α-Mg$[B_2(SO_4)_4]$ ("cation between layer"). It turned out that the experimental structure is less stable by 26.6 kJ mol^{-1}, thus predicting a possible α-modification.[13b] As shown above, we were able to synthesize exactly what was forecast by theory and additionally confirmed that by calculating the E–V diagrams. Again, the energy difference with PBE-D3 is less than what was obtained with a hybrid functional.[13b] Comparable to Mg$[B_2(SO_4)_4]$, the β-modification features a higher B_0 and therefore less compressibility.

The higher bulk modulus of the β-polymorphs might be explained by the interplay of three involved layers in the coordination environment on the metal cations. In contrast, in the α-polymorphs solely two layers are involved, leading to a slightly better compressibility.

Infrared spectroscopy

The infrared spectra of α-$M[B_2(SO_4)_4]$ and β-$M[B_2(SO_4)_4]$ (M = Mg, Co) are displayed in Figure 8 for the region 1800–400 cm^{-1} (full spectra in Figure S2 in the Supporting Information). Recently, IR modes for Ca$[B_2(SO_4)_4]$, comprising an analogous anionic structure,[5] were calculated and enabled assignment of the experimental data herein (Table S12 in the Supporting Information). The spectra of the α- and β-modification are very similar and only minor deviations occur, owing to minor deviations in the orientation of the tetrahedra in the crystal structure. For convenience, the bands of β-Co$[B_2(SO_4)_4]$ are discussed in the following. The asymmetric stretching mode $\nu_{asym.}$(S-O_{term}) can be found at 1195 cm^{-1}. The bands between 1170–1014 cm^{-1} can be assigned to asymmetric and symmetric stretching vibrations $\nu_{asym./sym.}$(B-O), followed by sym-

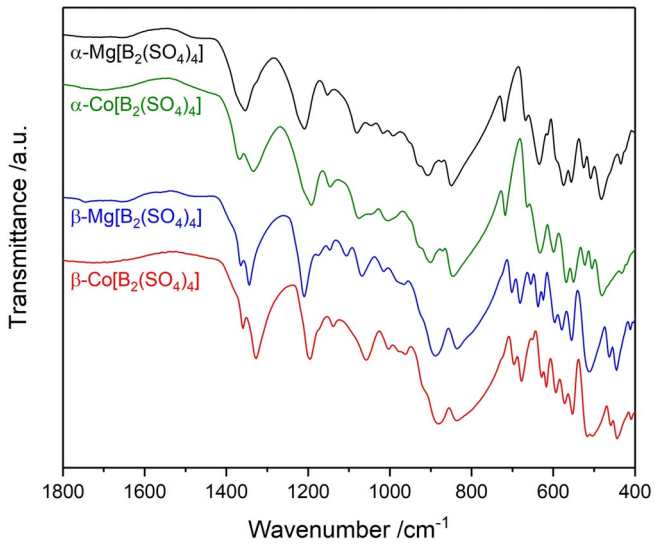

Figure 8. Infrared spectra of α-$M[B_2(SO_4)_4]$ (M = Mg (black), Co (green)) and β-$M[B_2(SO_4)_4]$ (M = Mg (blue), Co (red)).

metric stretching vibrations $\nu_{sym.}$(S-O) at 881 and 835 cm^{-1}. The asymmetric bending vibrations $\delta_{asym.}$(O-S-O, O-B-O, S-O-B) mainly occur between 696 and 553 cm^{-1}. The bands below result from asymmetric bending vibrations $\delta_{asym.}$(O-S-O, S-O-Co).

Optical spectroscopy

The powder reflectance spectra obtained for α- and β-$Co[B_2(SO_4)_4]$ (Figure 9) are very similar and typical for Co^{2+} ions in an almost undistorted octahedral oxoanionic coordination (cf. $[Co(OH_2)_6]^{2+}$ complex,[23] chromophore $[Co^{II}O_6]$ in CoP_4O_{11},[24] and many other anhydrous cobalt(II) phosphates[25]). Nevertheless, ligand field analyses following the procedure of Tanabe and Sugano[26] yield slightly different values for Δ_o and *B* for both modifications (Table 3). For α-$Co[B_2(SO_4)_4]$, a higher ligand field splitting and a lower value for the interelectronic repulsion parameter *B* are observed in comparison to the β-form. In this context, it is worth pointing out that the average distance $\acute{d}(Co\text{-}O)_\alpha = 207.3$ pm is shorter than $\acute{d}(Co\text{-}O)_\beta = 209.4$ pm. The same tendency, albeit less pronounced is obtained by DFT ($\acute{d}(Co\text{-}O)_\alpha = 205.8$ pm, $\acute{d}(Co\text{-}O)_\beta = 206.6$ pm). The ligand field parameters for the separately treated chromophores $[Co^{II}O_6]$ (all oxide ligands showing coordination number c.n.$(O^{2-}) = 2$, no bridging between two $[Co^{II}O_6]$) in α- and β-$Co[B_2(SO_4)_4]$ are comparable to those observed for CoP_4O_{11} (also "isolated" $[Co^{II}O_6]$). For the well-known hexa-aquo complex $[Co^{II}(OH_2)_6]^{2+}$ significantly higher Δ_o and smaller *B* values are reported in the literature (Table 3).[27] These differences are in line with the general assumption of a higher covalency and restraint π-bonding for the interaction Co-OH_2 (see: second sphere ligand field effects[28]). Weak shoulders on the higher and lower energy flank of the main absorption band, $^4T_{1g}(F) \rightarrow {}^4T_{1g}(P)$, are attributed to spin-forbidden transitions (Table 3) rather than to splitting of the spin-allowed transitions owing to low-symmetry components of the ligand fields around Co^{2+} in both modifications. This assignment is consistent with the Tanabe–Sugano evaluation.

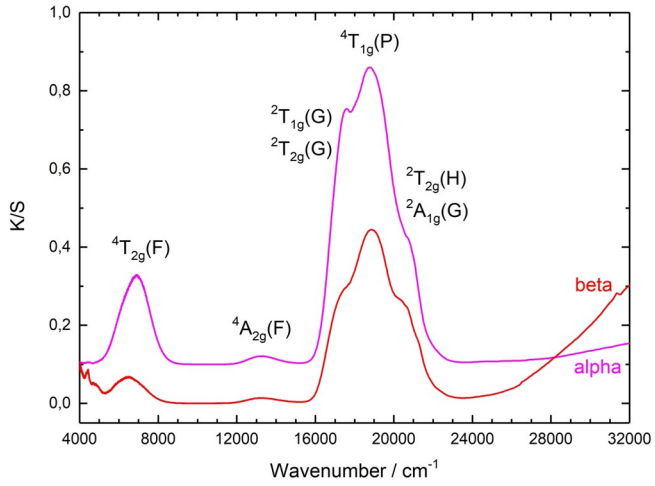

Figure 9. Powder reflectance spectra (UV/Vis/NIR region) of α-$Co[B_2(SO_4)_4]$ (magenta) and β-$Co[B_2(SO_4)_4]$ (red).

The powder reflectance spectra of α- and β-$Mg[B_2(SO_4)_4]$ both show a transition in the UV regime from the valence to the conduction band (Figures S4, S5 in the Supporting Information). An estimation of the band gaps was achieved by using a Tauc plot and yields similar values for both polymorphs with band gaps of 5.2(1) eV for α-$Mg[B_2(SO_4)_4]$ and 5.4(1) eV for β-$Mg[B_2(SO_4)_4]$. These figures are in line with calculations on the density of states revealing band gaps of 4.9 and 4.7 eV, respectively (Figure S3 in the Supporting Information). As expected for calculations using the PBE functional, the band gaps are slightly underestimated.

Thermal analysis

The thermal stability of α- and β-$Mg[B_2(SO_4)_4]$ was investigated under nitrogen atmosphere (Figure 10). Both phases show similar stabilities and start to decompose above 450 °C. The observed mass loss of 55.50 wt% (α) and 54.70 wt% (β) corresponds well to a calculated mass loss of 55.85 wt%, based on the release of three formula units of SO_3. Hence, α- and β-$Mg[B_2(SO_4)_4]$ decompose to $MgSO_4$ and B_2O_3 according to the following reaction [Eq. (1)]:

$$Mg[B_2(SO_4)_4] \rightarrow MgSO_4 + B_2O_3 + 3\,SO_3 \qquad (1)$$

Above 900 °C, $MgSO_4$ starts to partially decompose to MgO, which in situ reacts with B_2O_3 to give $Mg_2B_2O_5$. This is con-

Table 3. Electronic transitions of α- and β-$Co[B_2(SO_4)_4]$ and evaluation of the ligand field parameters Δ_o and *B* (according to Tanabe and Sugano). Data for CoP_4O_{11},[24] $CoSO_4$,[25] and the aquo-complex[27] $[Co(OH_2)_6]^{2+}$ are given for comparison.

	α-$Co[B_2(SO_4)_4]$	β-$Co[B_2(SO_4)_4]$	CoP_4O_{11}	$CoSO_4$	$[Co(OH_2)_6]^{2+}$
$^4T_{1g}(F) \rightarrow {}^4T_{2g}(F)$	6915	6528	7050	6528 7430 (6980)	8100
$^4T_{1g}(F) \rightarrow {}^4A_{2g}(F)$	13341	13341	13840	13800	16000
$^4T_{1g}(F) \rightarrow {}^2T_{2g}(G)$	17567	17485		17200	
$^4T_{1g}(F) \rightarrow {}^2T_{1g}(G)$					
$^4T_{1g}(F) \rightarrow {}^4T_{1g}(P)$	18773	18866	19100	19440 20224 (19832)	19400
$^4T_{1g}(F) \rightarrow {}^2A_{2g}(G)$	20587	20411	20410		
$^4T_{1g}(F) \rightarrow {}^2T_{2g}(H)$					
Δ_o	7958	7445	8145	8000	9200
B	853	896	873	933	850

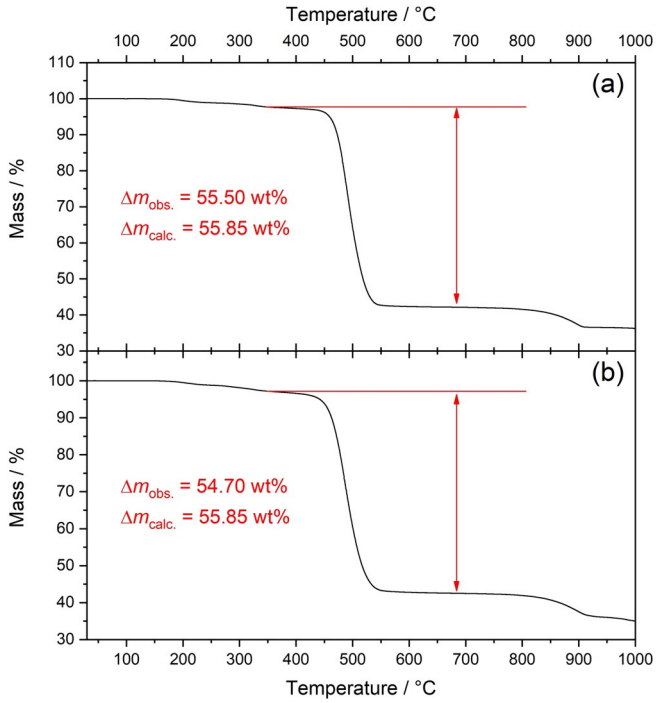

Figure 10. Thermal analysis of α-$Mg[B_2(SO_4)_4]$ (a) and β-$Mg[B_2(SO_4)_4]$ (b) under nitrogen atmosphere.

firmed by PXRD after the thermal analysis (Figure S6 in the Supporting Information). Thus, both compounds show a slightly lower thermal stability than $Mg_4[B_2O(SO_4)_6]$, comprising zero-dimensional anions,[9] which is expected to be due to the higher condensed network.[11]

Conclusion

Herein, we presented two new borosulfates, β-$Mg[B_2(SO_4)_4]$ and α-$Co[B_2(SO_4)_4]$, and characterized them together with the rather poorly characterized polymorph α-$Mg[B_2(SO_4)_4]$ as well as the polymorph β-$Co[B_2(SO_4)_4]$. The polymorphs were assigned based on the total electronic energies obtained from DFT calculations.

All structures comprise alternately corner-sharing borate and sulfate tetrahedra forming two-dimensional layers. Therein, the α- and β-polymorph differ by the position of the octahedrally coordinated metal cations. In the α-polymorph, these are located between the layers, whereas the cations in the β-polymorph are embedded within the layer, being coordinated in total by three adjacent layers.

Based on UV/Vis/NIR spectra of the two cobalt polymorphs, we were able to deduce ligand field splitting parameters as well as Racah parameters for 2D borosulfates for the very first time. Both polymorphs show a rather weak ligand field splitting and a weak covalency. Thus, these results are in line with our previous findings on transition metal and rare earth metal borosulfates.

Regarding the synthesis, a selective synthetic approach to the individual phases was made possible by carefully adjusting the oleum concentration during the synthesis. Presumably, the mixture of oleum and sulfuric acid—in addition with the extended time—might promote a direct formation of the borosulfate layers, so that the charge compensation is achieved by cations between these layers in the α-modification. In the β-modification, the formation of the borosulfate layers might be decelerated by the exclusive use of oleum and thus the formation of the borosulfate anions around the cations leads to embedded cations.

With this polymorph, we were able to prove experimentally the existence of the theoretically predicted α-$Co[B_2(SO_4)_4]$ phase and also extended this polymorph to β-$Mg[B_2(SO_4)_4]$. Based on our experimental data, DFT calculations confirmed the in silico experiments, yielding lower electronic energies in both cases for the α-modification, with cations residing between the layers.

This gained synthetic control in borosulfate chemistry enables a systematic access to phyllosilicate-analogous borosulfates and paves the way to the respective polymorphs for $M[B_2(SO_4)_4]$ (M = Mn, Ni, Zn).

Experimental Section

Synthesis

α- and β-$M[B_2(SO_4)_4]$ were synthesized by loading the metal carbonates $MgCO_3$ (42.1 mg, 0.5 mmol, Riedel de Haen) or $CoCO_3{\cdot}H_2O$ (68.4 mg, 0.5 mmol, Acros Organics) together with B_2O_3 (69.6 mg, 1 mmol, Sigma–Aldrich) in a silica glass ampoule (outer diameter: 1.2 cm, wall thickness: 0.1 cm, length: 12.5 cm). Subsequently, conc. sulfuric acid (0.5 mL) and oleum (0.5 mL, 65% SO_3, Merck) were added for the α-modification and oleum (1 mL) for the β-modification and the ampoule was torch sealed. For the α-modification, the fused ampoule was left for one day at room temperature. Eventually, the following temperature program was applied: heating to 453 K with 50 $K\,h^{-1}$, holding the temperature for 36 h, and cooling down to room temperature with 6 $K\,h^{-1}$.

Several single-crystals ($Mg[B_2(SO_4)_4]$: colorless; $Co[B_2(SO_4)_4]$: pink) were formed in the acid. The ampoules were opened after cooling down with liquid nitrogen. The excess acid was decanted and the crystals were washed with dry acetonitrile and vacuum filtrated. The compounds are sensitive to moisture and hence were transferred into an argon glovebox.

Crystal structure determination

Immediately after opening the ampoule, single crystals were transferred into perfluorinated polyether and selected for single-crystal XRD. Diffraction data for all compounds were collected with a Bruker D8 Venture diffractometer using $Mo_{K\alpha}$ radiation (λ = 0.71073 Å). The temperature was adjusted with a nitrogen flow (Oxford Cryosystems). The absorption correction was performed by employing the multi-scan method;[29] then, the crystal structures were solved with direct methods within the SHELXS program[30] and refined by the full-matrix least-squares technique within the SHELXTL program.[31] Further details of the crystal structure investigations discussed in this contribution are listed in Table 4 as well as Tables S1–S6 in the Supporting Information. Deposition Numbers 2014318 (α-$Co[B_2(SO_4)_4]$), CSD-2014319 (β-$Mg[B_2(SO_4)_4]$), and CSD-2014320 (β-$Co[B_2(SO_4)_4]$) contain the supplementary crystallographic data for this paper. These data are provided free of charge by the joint Cambridge Crystallographic Data Centre and Fachin-

Table 4. Crystal data and details of the structure refinements (esds in parentheses).

	α-Co[$B_2(SO_4)_4$]	β-Co[$B_2(SO_4)_4$]	β-Mg[$B_2(SO_4)_4$]
temperature [K]	250(2)	250(2)	200(2)
molar weight [g mol^{-1}]	464.79	464.79	430.17
crystal system	monoclinic	monoclinic	monoclinic
space group	*C*2/*c* (No. 15)	$P2_1/n$ (No. 14)	$P2_1/n$ (No. 14)
crystal size [mm^3]	0.23×0.15×0.05	0.13×0.11×0.06	0.05×0.02×0.01
a [pm]	1740.7(8)	795.3(5)	787.49(5)
b [pm]	534.3(3)	814.3(5)	807.76(5)
c [pm]	1433.4(10)	9.132(6)	904.75(5)
β [°]	125.926(12)	111.384(15)	111.4483(15)
volume [10^6 pm^3]	1079.5(10)	550.6(6)	535.66(6)
Z	4	2	2
$\rho_{calc.}$ [g cm^{-3}]	2.860	2.803	2.667
absorption coefficient μ [mm^{-1}]	2.472	2.423	1.055
F(000)	916	458	428
radiation (λ [pm])	71.073	71.073	71.073
absorption correction	multi-scan	multi-scan	multi-scan
index range *h*|*k*|*l* (min./max.)	−26/22|−8/8|−13/21	−12/12|−12/12|−13/13	−12/12|−13/13|−14/14
theta range [°]	$2.890 < \Theta < 32.500$	$2.915 < \Theta < 32.493$	$2.943 < \Theta < 32.044$
reflections collected	8191	15799	18444
independent reflections	1944	1988	2371
observed reflections ($I > 2\sigma$)	1703	1733	1948
R_{int}	0.0288	0.0404	0.0548
refined parameters	105	106	107
R_1 (all data)	0.0287	0.0280	0.0415
wR_2 (all data)	0.0585	0.0579	0.0746
GooF	1.039	1.070	1.094
residual electron density (min./max.) [e$^-$ Å^{-3}]	−0.462/0.599	−0.464/0.628	−0.535/0.704

formationszentrum Karlsruhe Access Structures service www.ccdc.cam.ac.uk/structures.

X-ray powder diffraction

The samples were ground and filled into a Hilgenberg glass capillary (outer diameter 0.3 mm, wall thickness 0.01 mm) inside a glovebox. The data was collected with a Bruker D8 Advance diffractometer with $Cu_{K\alpha}$ radiation ($\lambda = 1.54184$ Å) with a 1D LynxEye detector. Rietveld refinement was done by using the program TOPAS V.[32] Details on the Rietveld refinement are displayed in Table S7 (in the Supporting Information).

Infrared spectroscopy

The infrared spectra were recorded by using a Bruker EQUINOX 55 FTIR spectrometer equipped with a platinum ATR setup in the range 4000–400 cm^{-1}.

DFT calculations

Quantum chemical calculations were performed in the framework of density functional theory (DFT) by using a linear combination of Gaussian-type functions (LCGTF) scheme as implemented in CRYSTAL17.[33] Full structural optimizations were performed by using the PBE[34] xc-functional with D3 dispersion correction.[35] The convergence criterion was set to 10^{-8} a.u. All-electron basis sets for Mg, B, S, and O were taken from the literature.[36] The outermost coefficient for S was modified to 0.515. The convergence criterion considering the energy was set to 1×10^{-8} a.u. with a *k*-mesh sampling of 6×6×6. Energy–volume plots were fit to a Birch–Murnaghan equation of state. Vibrational frequencies were computed on the basis of the relaxed structures. Vibrational modes were visualized with the *J-ICE* application[37] and Jmol.[38]

Optical spectroscopy

The UV/Vis/NIR spectra for α- and β-Co[$B_2(SO_4)_4$] were measured with a PerkinElmer λ 750 s spectrometer in the range 250–2500 nm. The UV/Vis spectra for α- and β-Mg[$B_2(SO_4)_4$] were measured with a Varian Cary 300 Scan UV/Vis spectrophotometer in the range 200–800 nm.

Thermal analysis

The thermogravimetric analysis was done in alumina crucibles by employing a NETZSCH STA 409 PC Luxx in nitrogen atmosphere and a heating ramp of 10 K min^{-1}.

Acknowledgements

The authors thank the Deutsche Forschungsgemeinschaft (DFG) for financial support under the project HO 4503/5-1. P.N. thanks the Fonds der Chemischen Industrie (FCI) for a Ph.D. fellowship. F.P. thanks Prof. Bettina Lotsch, Dr. Ulrich Wedig, and the Computer Service group from the Max-Planck-Institute for Solid-State Research (Stuttgart, Germany) for access to CRYSTAL17 and computational facilities. Open access funding was enabled and organized by Projekt DEAL. Open access funding enabled and organized by Projekt DEAL.

Conflict of interest

The authors declare no conflict of interest.

Keywords: borosulfates · crystal structure · optical spectroscopy · polymorphism · silicate-analogs

[1] J. Bruns, H. A. Höppe, H. Hillebrecht, M. Daub, H. Huppertz, *Chem. Eur. J.* **2020**, *26*, 7966 – 7980.
[2] F. Liebau, *Structural Chemistry of Silicates*, Springer, Heidelberg, **1985**.
[3] H. A. Höppe, K. Kazmierczak, M. Daub, K. Förg, F. Fuchs, H. Hillebrecht, *Angew. Chem. Int. Ed.* **2012**, *51*, 6255 – 6257; *Angew. Chem.* **2012**, *124*, 6359 – 6362.
[4] M. Daub, K. Kazmierczak, P. Gross, H. Höppe, H. Hillebrecht, *Inorg. Chem.* **2013**, *52*, 6011 – 6020.
[5] J. Bruns, M. Podewitz, M. Schauperl, B. Joachim, K. R. Liedl, H. Huppertz, *Chem. Eur. J.* **2017**, *23*, 16773 – 16781.
[6] a) P. Gross, A. Kirchhain, H. A. Höppe, *Angew. Chem. Int. Ed.* **2016**, *55*, 4353 – 4355; *Angew. Chem.* **2016**, *128*, 4426 – 4428; b) P. Netzsch, P. Gross, H. Takahashi, S. Lotfi, J. Brgoch, H. A. Höppe, *Eur. J. Inorg. Chem.* **2019**, 3975 – 3981; c) M. Daub, H. Hillebrecht, *Eur. J. Inorg. Chem.* **2015**, 4176 – 4181.
[7] M. Daub, K. Kazmierczak, H. A. Höppe, H. Hillebrecht, *Chem. Eur. J.* **2013**, *19*, 16954 – 16962.
[8] a) T. Jüstel, H. Nikol, C. Ronda, *Angew. Chem. Int. Ed.* **1998**, *37*, 3084 – 3103; *Angew. Chem.* **1998**, *110*, 3250 – 3271; b) H. A. Höppe, *Angew. Chem. Int. Ed.* **2009**, *37*, 3572 – 3582; *Angew. Chem.* **2009**, *121*, 3626 – 3636; c) Y. C. Lin, M. Karlsson, M. Bettinelli in *Photoluminescent Materials and Electroluminescent Devices. Topics in Current Chemistry Collections* (Eds.: N. Armaroli, H. Bolink), Springer, Cham, **2017**, pp. 309-355; ; d) M. Sato, S. W. Kim, Y. Shimomura, T. Hasegawa, K. Toda, G. Adachi, *Handbook on the Physics and Chemistry of Rare Earths* **2016**, *49*, 1 – 128; e) N. C. George, K. A. Denault, R. Seshadri, *Annu. Rev. Mater. Res.* **2013**, *43*, 481 – 501.
[9] P. Netzsch, P. Gross, H. Takahashi, H. A. Höppe, *Inorg. Chem.* **2018**, *57*, 8530 – 8539.
[10] a) A. Leclaire, M. Lamire, B. Raveau, *Acta Crystallogr. Sect. C* **1988**, *44*, 1181 – 1184; b) M. Schöneborn, Dissertation, Rheinischen Friedrich-Wilhelms-Universität Bonn, Germany, **2008**; c) R. Glaum, Dissertation, Justus-Liebig-Universität, Germany, **1990**.
[11] P. Netzsch, M. Hämmer, P. Gross, H. Bariss, T. Block, L. Heletta, R. Pöttgen, J. Bruns, H. Huppertz, H. A. Höppe, *Dalton Trans.* **2019**, *48*, 4387 – 4397.
[12] C. Logemann, M. S. Wickleder, *Angew. Chem. Int. Ed.* **2013**, *52*, 14229 – 14232; *Angew. Chem.* **2013**, *125*, 14479 – 14482.
[13] a) L. C. Pasqualini, H. Huppertz, J. Bruns, *Inorganics* **2019**, *7*, 145; b) L. Pasqualini, O. Janka, S. Olthof, H. Huppertz, K. Liedl, R. Pöttgen, M. Podewitz, J. Bruns, *Chem. Eur. J.* **2020**, https://doi.org/10.1002/chem.202002221.
[14] W. Loewenstein, *Am. Mineral.* **1954**, *39*, 92 – 96.
[15] P. Netzsch, H. A. Höppe, *Z. Anorg. Allg. Chem.* **2020**, https://doi.org/10.1002/zaac.202000105.
[16] a) T. Balić Žunić, E. Makovicky, *Acta Crystallogr. Sect. B* **1996**, *52*, 78 – 81; b) E. Makovicky, T. Balić-Žunić, *Acta Crystallogr. Sect. B* **1998**, *54*, 766 – 773.
[17] R. W. G. Wyckoff, *Am. J. Sci.* **1925**, *s5-9*, 448 – 459.
[18] J. Peters, B. Krebs, *Acta Crystallogr. Sect. B* **1982**, *38*, 1270 – 1272.
[19] R. D. Shannon, *Acta Crystallogr. Sect. A* **1976**, *32*, 751 – 767.
[20] a) R. Hoppe, *Angew. Chem. Int. Ed.* **1966**, *5*, 95 – 106; *Angew. Chem.* **1966**, *78*, 52 – 63; b) R. Hoppe, *Angew. Chem. Int. Ed. Engl.* **1970**, *9*, 25 – 34; *Angew. Chem.* **1970**, *82*, 7 – 16; c) R. Hübenthal, *MAPLE*: Program for the Calculation of the Madelung Part of Lattice Energy, Universität Gießen, Germany, **1993**.
[21] T. Kato, Y. Takéuchi, *Can. Mineral.* **1983**, *21*, 1 – 6.
[22] J. S. Knyrim, F. Roessner, S. Jakob, D. Johrendt, I. Kinski, R. Glaum, H. Huppertz, *Angew. Chem. Int. Ed.* **2007**, *46*, 9097 – 9100; *Angew. Chem.* **2007**, *119*, 9256 – 9259.
[23] B. N. Figgis, M. A. Hitchman, *Ligand Field Theory and its Applications*, Wiley-VCH, New York, NY, **2000**.
[24] M. Funke, R. Glaum, *unpublished results*.
[25] A. Schmidt, Dissertation, Justus-Liebig-Universität, Germany, **2002**.
[26] a) Y. Tanabe, S. Sugano, *J. Phys. Soc. Jpn.* **1954**, *9*, 753 – 766; b) Y. Tanabe, S. Sugano, *J. Phys. Soc. Jpn.* **1954**, *9*, 766 – 779.
[27] A. B. P. Lever, *Inorganic Electronic Spectroscopy*, Elsevier, Amsterdam, Netherlands, **1984**.
[28] D. Reinen, M. Atanasov, S.-L. Lee, *Coord. Chem. Rev.* **1998**, *175*, 91 – 158.
[29] Bruker, *SADABS*; Bruker AXS Inc, Madison, Wisconsin, USA, **2001**.
[30] G. M. Sheldrick, *Acta Crystallogr. Sect. A* **2008**, *64*, 112 – 122.
[31] G. M. Sheldrick, *Acta Crystallogr. Sect. C* **2015**, *71*, 3 – 8.
[32] Bruker, *Topas V5*: General profile and structure analysis software for powder diffraction data, Karlsruhe, Germany, **2014**.
[33] a) R. Dovesi, A. Erba, R. Orlando, C. M. Zicovich-Wilson, B. Civalleri, L. Maschio, M. Rerat, S. Casassa, J. Baima, S. Salustro, B. Kirtman, *WIREs Comput. Mol. Sci.* **2018**, *8*, e1360; b) R. Dovesi, V. R. Saunders, C. Roetti, R. Orlando, C. M. Zicovich-Wilson, F. Pascale, B. Civalleri, K. Doll, N. M. Harrison, I. J. Bush, P. D'Arco, M. Llunell, M. Causà, Y. Noël, L. Maschio, A. Erba, M. Rerat, S. Casassa, *CRYSTAL17*: User's Manual; University of Torino, Torino, **2017**.
[34] J. P. Perdew, K. Burke, M. Ernzerhof, *Phys. Rev. Lett.* **1996**, *77*, 3865.
[35] a) S. Grimme, A. Hansen, J. G. Brandenburg, C. Bannwarth, *Chem. Rev.* **2016**, *116*, 5105 – 5154; b) S. Grimme, J. Antony, S. Ehrlich, H. Krieg, *J. Chem. Phys.* **2010**, *132*, 154104; c) S. Grimme, S. Ehrlich, L. Goerigk, *J. Comput. Chem.* **2011**, *32*, 1456 – 1465.
[36] a) L. Valenzano, Y. Noël, R. Orlando, C. M. Zicovich-Wilson, M. Ferrero, R. Dovesi, *Theor. Chem. Acc.* **2007**, *117*, 991 – 1000; b) R. Dovesi, F. Freyria Fava, C. Roetti, V. R. Saunders, *Faraday Disc.* **1997**, *106*, 173 – 187; c) R. Orlando, R. Dovesi, C. Roetti, *J. Phys. Condens. Matter* **1990**, *2*, 7769 – 7789; d) A. Lichanot, E. Aprà, R. Dovesi, *Phys. Status Solidi B* **1993**, *177*, 157 – 163; e) J. Scaranto, S. Giorgianni, *J. Mol. Struct.* **2008**, *858*, 72 – 76.
[37] P. Canepa, R. M. Hanson, P. Ugliengo, M. Alfredsson, *J. Appl. Crystallogr.* **2011**, *44*, 225 – 229.
[38] Jmol: An open-source Java viewer for chemical structures in 3D, http://www.jmol.org/.

Manuscript received: July 7, 2020
Accepted manuscript online: August 3, 2020
Version of record online: October 7, 2020